CHEMISTRY OF MATERIALS

ARTICLE

pubs.acs.org/cm

Crystallization and Phase-Transition Characteristics of Sol−Gel-Synthesized Zinc Titanates

Nicholas T. Nolan,[†,‡] Michael K. Seery,[†] and Suresh C. Pillai*[,‡]

[†]School of Chemical and Pharmaceutical Sciences, Dublin Institute of Technology, Kevin Street, Dublin 8, Ireland and

[‡]Centre for Research in Engineering Surface Technology (CREST), Focas Institute, Dublin Institute of Technology, Kevin Street, Dublin 8, Ireland

ABSTRACT: The synthesis of a $ZnO-TiO_2$ nanocomposite usually results in the formation of one or more of three compounds—Zn_2TiO_4, $Zn_2Ti_3O_8$, and $ZnTiO_3$—along with other secondary impurity phases, such as rutile-TiO_2 or ZnO. Obtaining a phase-pure composite of either of these materials is one of the challenges in materials chemistry. For example, pure $ZnTiO_3$ cannot be synthesized under normal conditions, because the $ZnTiO_3$ phase readily transforms to Zn_2TiO_4 and rutile. $Zn_2Ti_3O_8$ is reported as a metastable form of $ZnTiO_3$. The Zn_2TiO_4 form is usually synthesized via solid-state reaction at high temperatures (typically above 1000 °C). In the current study, the crystalline and phase-transformation behaviors of sol−gel-synthesized zinc titanates has been investigated systematically, with regard to various Zn:Ti precursor molar ratios. X-ray diffraction (XRD) has shown that, with excess titanium precursor, zinc metatitanate ($ZnTiO_3$) is the preferred zinc titanate phase formed at temperatures of 600−900 °C, with a direct transformation of zinc metatitanate to zinc orthotitanate (Zn_2TiO_4) occurring at 1000 °C. However, synthesis involving titanium precursor in the presence of excess zinc precursor forms $Zn_2Ti_3O_8$ with a cubic defect spinel structure at temperatures of 700−900 °C, with a direct transformation to zinc orthotitanate occurring at 1000 °C. The current study also indicated that the percentage of zinc titanate phases can be controlled by varying the initial sol−gel reaction conditions. Spectroscopic investigations have been carried out to understand the effect of precursor ($Zn(CH_3COO)_2 \cdot 2H_2O$ and $H_2C_2O_4$) formulations on the crystallization and phase-transition behaviors of these composites. Fourier transform infrared and Raman spectroscopy have shown the presence of the oxalate form of zinc and titanium. However, neither of these techniques could reveal if the titanium oxalate chains exist separately from zinc oxalate chains or if they combine during the initial stages of preparation. Further powder XRD investigation proposed that two separate metal oxalate chains were formed during the synthesis. Previous reports indicate that the formation of Zn_2TiO_4 and $Zn_2Ti_3O_8$ is limited by the presence of anatase and $ZnTiO_3$ only forms in the presence of rutile. Results from the present study confirm that, in a sol−gel synthesis, the formation of various forms of zinc titanates is influenced by the zinc oxide/titanium dioxide composition.

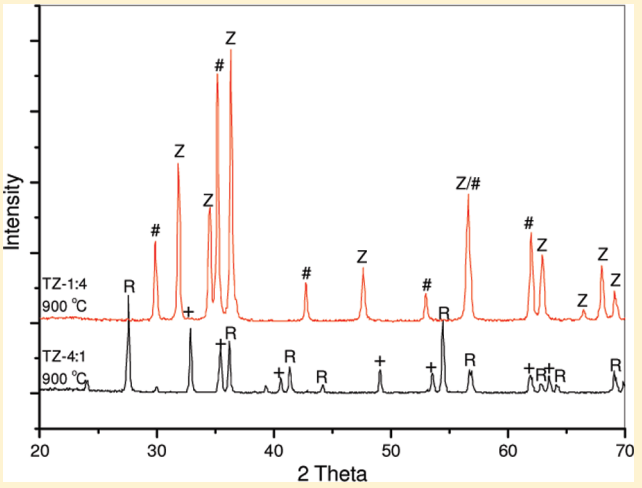

KEYWORDS: composites (including ceramic composites), crystal growth, inorganic solids and ceramics

INTRODUCTION

Semiconductor research has recently shown great promise recently in areas such as hydrogen production through photocatalytic water splitting,[1] dye-sensitized solar cells,[2] and photocatalytic remediation of harmful organics from air and water.[3,4] Of the semiconductors investigated, titanium dioxide (TiO_2) has received the most attention, because of its excellent stability, nontoxicity, cost, and availability, as well as its ability to produce highly oxidizing radicals.[5,6] Zinc oxide (ZnO) has also shown promise in the areas of solar cells,[7] gas sensors,[8,9] and photocatalysis.[10]

The simultaneous synthesis of a $ZnO-TiO_2$ composite usually results in the formation of one or more of the three known compounds from the $ZnO-TiO_2$ system: Zn_2TiO_4 (zinc orthotitanate), with a cubic spinel crystal structure; $Zn_2Ti_3O_8$, with a cubic defect spinel structure; and $ZnTiO_3$ (zinc metatitanate), with a rhombohedral ilmenite structure.[11−14] $Zn_2Ti_3O_8$ is the metastable, low-temperature (<820 °C) form of $ZnTiO_3$;[14] however, pure $ZnTiO_3$ is not easily obtained, because it transforms to Zn_2TiO_4 and rutile.[12,13]

Zinc orthotitanate (Zn_2TiO_4) is an inverse spinel that has been used as a catalyst and a pigment.[15] As a catalyst, $ZnTiO_4$ is used as a sorbent for the removal of sulfur from coal gasification product gases, in hot gas desulfurization units, at temperatures in the range of 400−700 °C. Zinc orthotitanate can easily withstand these temperatures, but it is also one of the leading regenerable catalysts.[15−21] Zn_2TiO_4 may also be used for the photocatalytic

Received: November 4, 2010
Revised: February 2, 2011
Published: February 28, 2011

Table 1. Molar Ratios and Amounts of Reactants Used for the Synthesis of Powders

sample ID	Ti:Zn	ZnAcOH (g)	EtOH (mL)	oxalic acid (g)	EtOH (mL)	TTIP (mL)	H_2O (mL)
TZ-4:1	0.0500:0.0125	2.29	125	3.15	50	14.80	90.00
TZ-4:2	0.0500:0.0250	4.58	250	6.30	100	14.80	90.00
TZ-4:3	0.0500:0.0375	6.88	375	9.45	150	14.80	90.00
TZ-1:4	0.0125:0.0500	9.17	500	12.60	200	3.70	22.50
TZ-2:4	0.0250:0.0500	9.17	500	12.60	200	7.40	45.00
TZ-3:4	0.0375:0.0500	9.17	500	12.60	200	11.10	67.50

splitting of water and the photocatalytic degradation of organic compounds.[22] Like other semiconductor photocatalysts, Zn_2TiO_4 has a wide band gap (3.1 eV), restricting its photocatalytic activity to ultraviolet (UV) light.[22,23] It is usually synthesized via solid-state reaction at high temperatures and typically, when a temperature below 1000 °C is used, longer heat treatments times are required.[15,16,18,20,24] Alternative synthesis methods have been employed such as the coprecipitation method. Heat treatment at 700 °C for 2 h resulted in the formation of zinc orthotitanate, but secondary phases were also present.[17] A single-phase material was obtained by Lew et al., using the citrate method followed by heat treatment at 720 °C for 12 h.[19] Spinel-type Zn_2TiO_4 was prepared by solid-state reaction of ZnO and TiO_2 in molar ratios of 3:2 at 1350 °C.[25,26]

In the present study, a range of ratios of titanium and zinc precursors has been synthesized. The calcined powders were investigated by X-ray diffraction (XRD), and, to investigate the molecular structure of the amorphous samples, Fourier transform infrared (FTIR) and Raman spectroscopic techniques were employed. At optimum molar ratios, pure Zn_2TiO_4 was formed under low heating temperatures (1000 °C) for short periods of time (2 h).

EXPERIMENTAL SECTION

Zinc acetate dihydrate (98%), titanium tetraisopropoxide (TTIP, 97%), and oxalic acid (98.5%) were all purchased from Aldrich and used without further purification. Ethanol (99.5%) was purchased from VWR International and used as received. Deionized water was used in all experimental techniques. In a typical synthesis, zinc acetate (9.17 g) was dissolved in ethanol (500 mL) at 60 °C. Oxalic acid (12.6 g) dissolved in ethanol (200 mL) was then added slowly to the zinc acetate solution to give a white, cloudy gel-like suspension. To the resulting white cloudy suspension, TTIP (11.10 mL) was added, immediately followed by water (67.50 mL). This resulted in a Ti:Zn molar ratio of 0.0375:0.05. The suspension was stirred for 2 h before being aged in an oven in air at 100 °C for 48 h to evaporate excess solvent. The resulting xerogel was then calcined at 400, 500, 600, 700, 800, 900, and 1000 °C for 2 h at a ramp rate of 5 °C/min. The synthesis was repeated for six different molar ratios (see Table 1).

A Siemens D 500 X-ray diffractometer, with a diffraction angle range of $2\theta = 20°-80°$, using Cu Kα radiation, was used to collect XRD diffractograms. Quantitative phase analysis was estimated by comparing the integrated diffraction peaks from the different phases, as described elsewhere.[27]

The crystallite size (T) was estimated (±5%) using the Scherrer equation (eq 1):[28,29]

$$T = \frac{0.9\lambda}{\beta \cos \theta} \quad (1)$$

where T is the crystallite size, λ the X-ray wavelength, θ the Bragg angle, and β the full width at half maximum (fwhm). Infrared spectra were recorded on a Perkin−Elmer GX FTIR spectrometer and recorded as a KBr disk (1:10, sample/KBr). A Horiba Jobin−Yvon LabRAM HR Raman system was used to obtain Raman spectra, employing a laser excitation wavelength of 532 nm.

RESULTS

X-ray Diffraction. *Excess Titanium Precursor.* The calculated phase compositions of samples TZ-4:1, TZ-4:2, and TZ-4:3 are shown in Figures 1a, 1b, and 1c, respectively. The phase compositions were calculated from the largest non-overlapping peaks of the representative phases from the X-ray diffractograms.

Sample TZ-4:1 has the greatest excess of titanium precursor, when compared with the other samples. This is clearly reflected in the composition of the phases. Titanium dioxide morphologies are the majority structure type at all temperatures. Anatase dominates at temperatures of 400−600 °C, and rutile is the predominant phase at 700−1000 °C. At calcination temperatures of 400 and 500 °C, TiO_2 (87%) and ZnO (13%) exist separately. At 600 °C, the metastable zinc metatitanate (7%, $ZnTiO_3$)[30] begins to form, and the crystallization of zinc metatitanate then accelerates as the temperature increases. At 700, 800, and 900 °C, the sample is composed of 30%−40% zinc metatitanate. Traces of the cubic spinel $Zn_2Ti_3O_8$ (2%−3%) can be found at 800 and 900 °C; at 1000 °C, zinc orthotitanate (42%) and rutile are the only phases present.

Crystallite sizes of the samples calcined at 400 and 500 °C, which consist of only anatase and zinc oxide, were calculated from the X-ray diffractograms using the Scherrer equation. For samples TZ-4:1, TZ-4:2, and TZ-4:3, anatase crystal sizes from 7 nm (at 400 °C) to 10 nm (at 500 °C) were calculated. Zinc oxide was also present at temperatures of 400−500 °C, and crystal sizes of 13−15 nm were calculated for zinc oxide. No ZnO crystal growth was found when the temperature was increased from 400 °C to 500 °C.

As the amount of zinc precursor is increased (TZ-4:2 and TZ-4:3), the titania phase concentration is reduced and the amount of zinc titanates present increases, as expected. As shown with sample TZ-4:1, sample TZ-4:2 at 400 and 500 °C consists of only anatase (85%) and zinc oxide. As the temperature increases, zinc titanates begin to form. At 600 °C, rutile is present for sample TZ-4:1, but rutile does not form until 700 °C for samples TZ-4:2 and TZ-4:3, which indicates that increased amounts of zinc precursor delay the anatase-to-rutile transformation, which is opposite to that observed by Liu et al.[30] Samples TZ-4:2 and TZ-4:3 also contain anatase at 700 °C, but sample TZ-4:1 does not, thus providing further evidence that increased amounts of zinc precursor delay the anatase-to-rutile transformation. Increased amounts of zinc precursor also promote the formation of the cubic spinel $Zn_2Ti_3O_8$ structure. For TZ-4:1, the cubic spinel $Zn_2Ti_3O_8$ forms at 800 °C (3%), $Zn_2Ti_3O_8$ is seen at 700 °C with sample TZ-4:2 (9%) and $Zn_2Ti_3O_8$ forms at 600 °C for sample TZ-4:3 (12%). Also, as can be expected, at 1000 °C, all samples consist of only zinc orthotitanate and rutile.

dx.doi.org/10.1021/cm1031688 |Chem. Mater. 2011, 23, 1496–1504

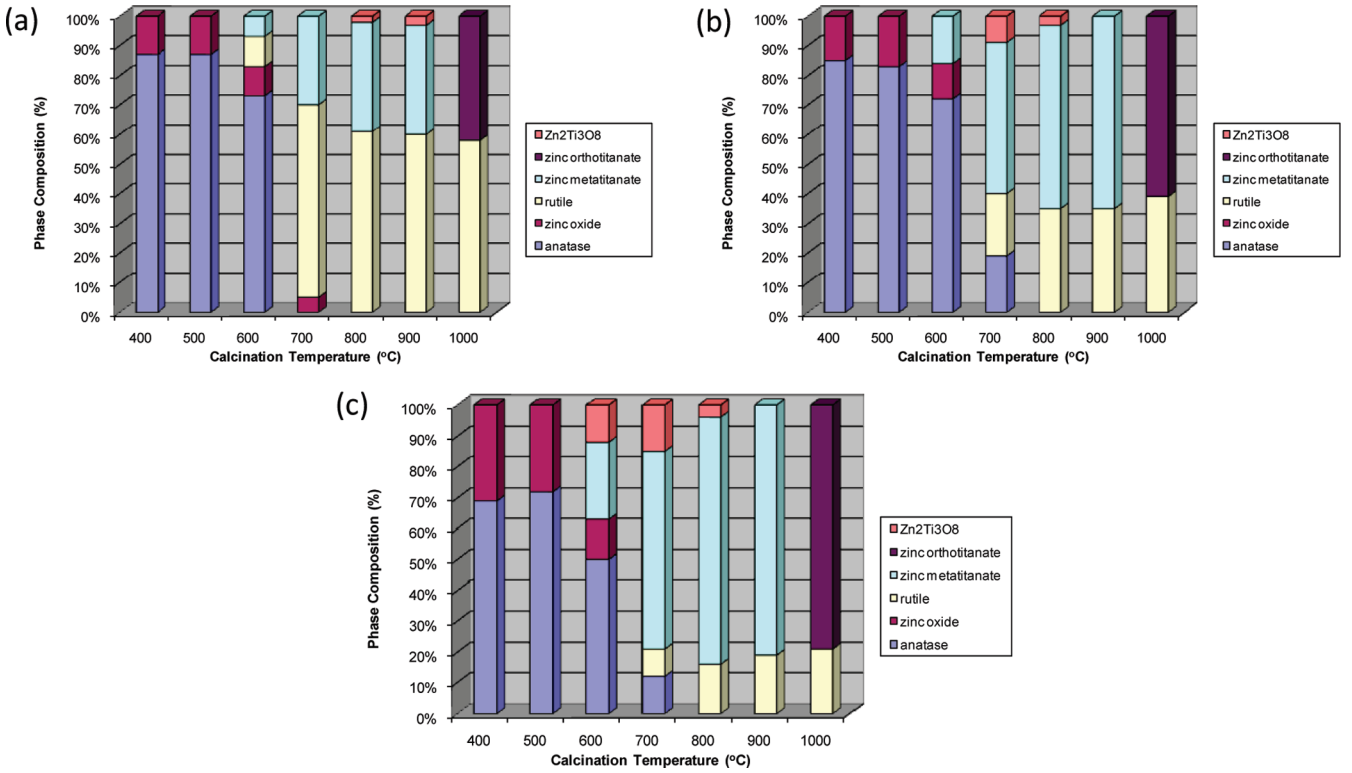

Figure 1. Phase compositions of (a) sample TZ-4:1, (b) sample TZ-4:2, and (c) sample TZ-4:3.

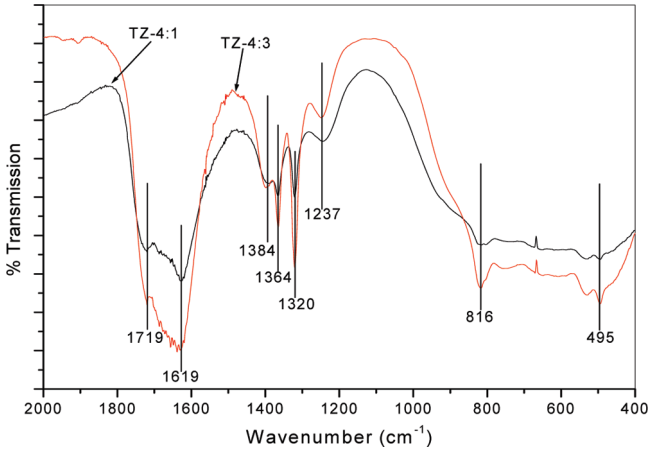

Figure 2. Infrared (IR) spectra of samples TZ-4:1 and TZ-4:3.

As the amount of zinc precursor is increased, the amount of zinc orthotitanate is also increased in an almost-linear manner. For the samples calcined at 1000 °C, a Ti:Zn ratio of 4:1 gives a 60/40 rutile/zinc orthotitanate composition, a Ti:Zn ratio of 4:2 gives a 40/60 rutile/zinc orthotitanate composition, and a Ti:Zn ratio of 4:3 gives a 20/80 rutile/zinc orthotitanate composition. A similar pattern is also observed for zinc metatitanate, but other phases ($Zn_2Ti_3O_8$) also are present. For all samples, the percentage of zinc metatitanate at 800 and 900 °C was almost identical to the amount of zinc orthotitanate at 1000 °C, indicating a direct transformation from zinc metatitanate to zinc orthotitanate.

Infrared Spectroscopy. Figure 2 shows the IR spectra of samples TZ-4:1 and TZ-4:3 before calcination. The assigned signals are summarized in Table 2. The zinc oxalate signals are in agreement with the data reported by Gabal et al.[31] Asymmetric

Table 2. Assigned Frequencies for IR Spectra of TZ-4:1 and TZ-4:3

observed frequency (cm^{-1})	assignment
1719	$\nu_{asym}(COO^-)$ titanium oxalate
1619	$\nu_{asym}(COO^-)$ zinc oxalate
1384	$\nu_{sym}(COO^-)$ titanium oxalate
1364	$\nu_{sym}(COO^-)$ zinc oxalate
1320	$\nu_{sym}(COO^-)$ zinc oxalate
1237	$\nu_{sym}(COO^-)$ titanium oxalate
816	$\delta_{asym}(O-C-O)$ zinc oxalate
495	$\nu(M-O)$ and $\delta_{asym}(C-C-O)$ zinc oxalate

($1719\ cm^{-1}$) and symmetric carboxylate stretches (1384 and $1237\ cm^{-1}$) are assigned to titanium oxalate. Comparing the IR spectra shown in Figure 2, the presence of additional amounts of zinc causes an increase in the zinc oxalate $\nu_{asym}(COO^-)$ stretch at $1619\ cm^{-1}$, relative to its titanium oxalate equivalent at $1719\ cm^{-1}$. There is also an increase in the $\nu_{sym}(COO^-)$ stretches of zinc oxalate (1364 and $1320\ cm^{-1}$), compared to their titanium counterpart (1384 and $1237\ cm^{-1}$). These results are to be expected, because an increase in zinc oxalate is going to provide an increase in the resulting peak intensities. Therefore, the initial amounts of titanium and zinc will control the composition of the metal oxalate chain. Any infrared features typical of Ti-OR coordination bonds[32] are not present in Figure 2, suggesting that a polymeric zinc/titanium oxalate exists where OR groups have been removed.[32]

Raman Spectroscopy. Figure 3 shows the Raman spectra of samples TZ-4:1 and TZ-4:3 where titanium is in excess. The range of $0-1000\ cm^{-1}$ represents the M−O stretches of the molecule. Peaks at 158, 418, 540, and $643\ cm^{-1}$ are similar to

dx.doi.org/10.1021/cm1031688 |*Chem. Mater.* 2011, 23, 1496–1504

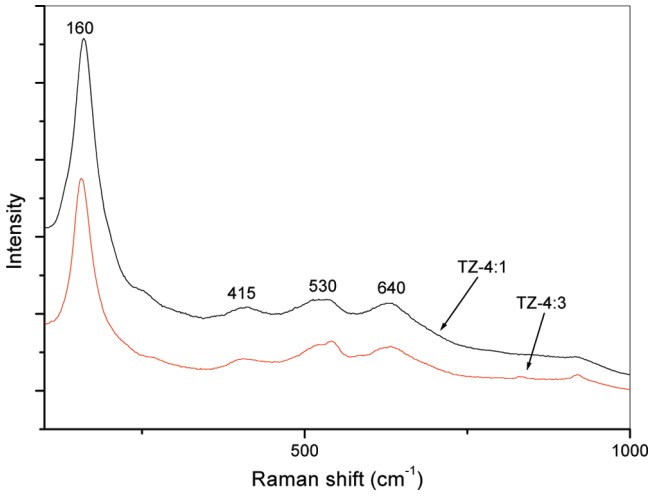

Figure 3. Raman spectra of samples TZ-4:1 and TZ-4:3.

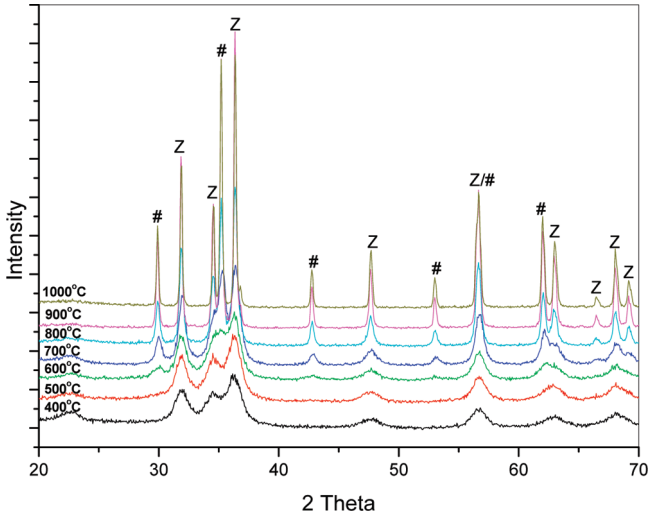

Figure 4. XRD of sample TZ-1:4 (peak identifications: (Z) ZnO and (#) $Zn_2Ti_3O_8$) at 600−900 °C, and $TiZn_2O_4$ at 1000 °C.

those of the anatase four-peak pattern.[33−35] During the crystallization process, titanium hydrolysate forms anatase/rutile-like structures that can be detected using Raman spectroscopy. These Raman spectral patterns then disappear before the material crystallizes to anatase.[35] Raman studies show that Ti−O structures are dominating the metal oxide framework during the early processes of the reaction. This is expected as the titanium precursor is in excess over that of the zinc precursor. When the zinc precursor exceeds the titanium precursor, Raman spectra with different spectral profiles are obtained.

Excess Zinc Precursor

XRD. The X-ray diffractogram of sample TZ-1:4 (Figure 4) shows that ZnO is the only crystal structure present at temperatures 400 and 500 °C. $Zn_2Ti_3O_8$ begins to form at 600 °C, and in the range of 700−900 °C, the $Zn_2Ti_3O_8$ and zinc oxide peak intensities grow stronger, indicating an increase in crystallinity for both phases. At 1000 °C, $Zn_2Ti_3O_8$ transforms to zinc orthotitanate, with zinc oxide also being present. There are no TiO_2 phases present at any temperature.

As the amount of titanium precursor was increased (sample TZ-3:4), anatase is present, along with zinc oxide at calcination temperatures of 400 and 500 °C (see Figure 5). At 600 and 700 °C,

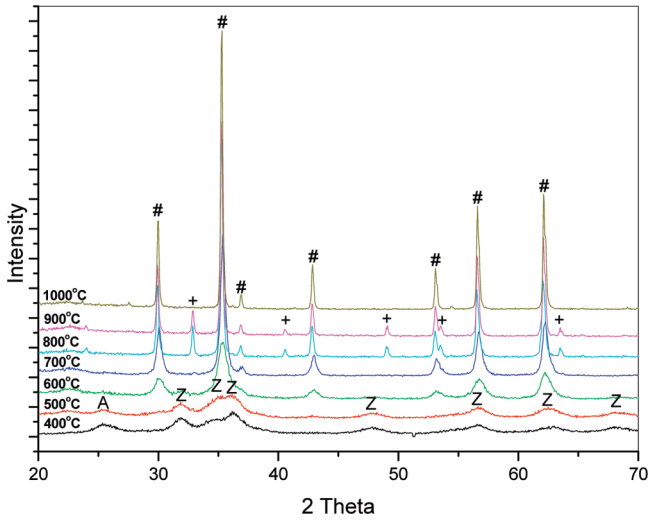

Figure 5. XRD spectra of sample TZ-3:4 (peak identifications: (A) anatase, (Z) ZnO, (+) $ZnTiO_3$, and (#) $Zn_2Ti_3O_8$) at 600−900 °C, and $TiZn_2O_4$ at 1000 °C.

the metastable $Zn_2Ti_3O_8$ is the only phase present. At 800 °C, zinc metatitanate forms along with $Zn_2Ti_3O_8$, and, at 900 °C, the sample consists of zinc metatitanate and either $Zn_2Ti_3O_8$ or zinc orthotitanate. (This is unclear, because of similarities in the X-ray inflections.) At 1000 °C, zinc orthotitanate is the dominant phase with trace amounts (3%) of rutile being present.

Figures 6a, 6b, and 6c summarizes the compositions for samples TZ-1:4, TZ-2:4, and TZ-3:4, respectively. For lower calcination temperatures (400−600 °C), the primary zinc oxide peak was overlapping with the $Zn_2Ti_3O_8$ (and zinc orthotitanate peak and, as such, the composition percentages could not be determined at temperatures of 400−600 °C. However, from the XRD diffractograms (Figure 4 and 5), zinc oxide is the only phase present at temperatures of 400 and 500 °C for sample TZ-1:4 (Figure 4) and the same was seen for sample TZ-2:4, however, Figure 5 (sample TZ-3:4) shows that both anatase and zinc oxide are present at 400 and 500 °C, while at 600 and 700 °C, only the metastable $Zn_2Ti_3O_8$ exists. Figures 6a−c show that the amount of $Zn_2Ti_3O_8$ increases as the amount of titanium precursor increases at temperatures of 700−900 °C. Results infer that $Zn_2Ti_3O_8$ directly transforms to zinc orthotitanate without affecting the zinc oxide crystal, as can be seen for samples TZ-1:4 and TZ-2:4 (see Figures 6a and 6b). Results for sample TZ-3:4 (see Figure 6c) indicate the same direct transformation from $Zn_2Ti_3O_8$ to zinc orthotitanate with the minor phase, zinc metatitanate, transforming to rutile.

Titanium dioxide and zinc oxide crystal size was determined from X-ray diffractograms, using the Scherrer equation. Sample TZ-1:4 consisted of ZnO only, but an anatase crystal size of 7 nm was found for samples TZ-2:4 and TZ-3:4 when calcined at 400 °C. At 500 °C, the anatase crystal grains grew to 10 nm. No crystal size growth was found for ZnO with crystal sizes of 13−15 nm calculated for samples TZ-2:4 and TZ-3:4 at 400 and 500 °C.

Calculated crystal sizes for samples with excess zinc precursor duplicated the results found for samples where excess titanium precursor was used. Therefore, it was shown that crystallite size has no significant influence over the transformation behavior of the zinc titanate materials.

The results show that almost-identical amounts of $Zn_2Ti_3O_8$ transform to zinc orthotitanate when the amount of zinc

dx.doi.org/10.1021/cm1031688 |*Chem. Mater.* 2011, 23, 1496–1504

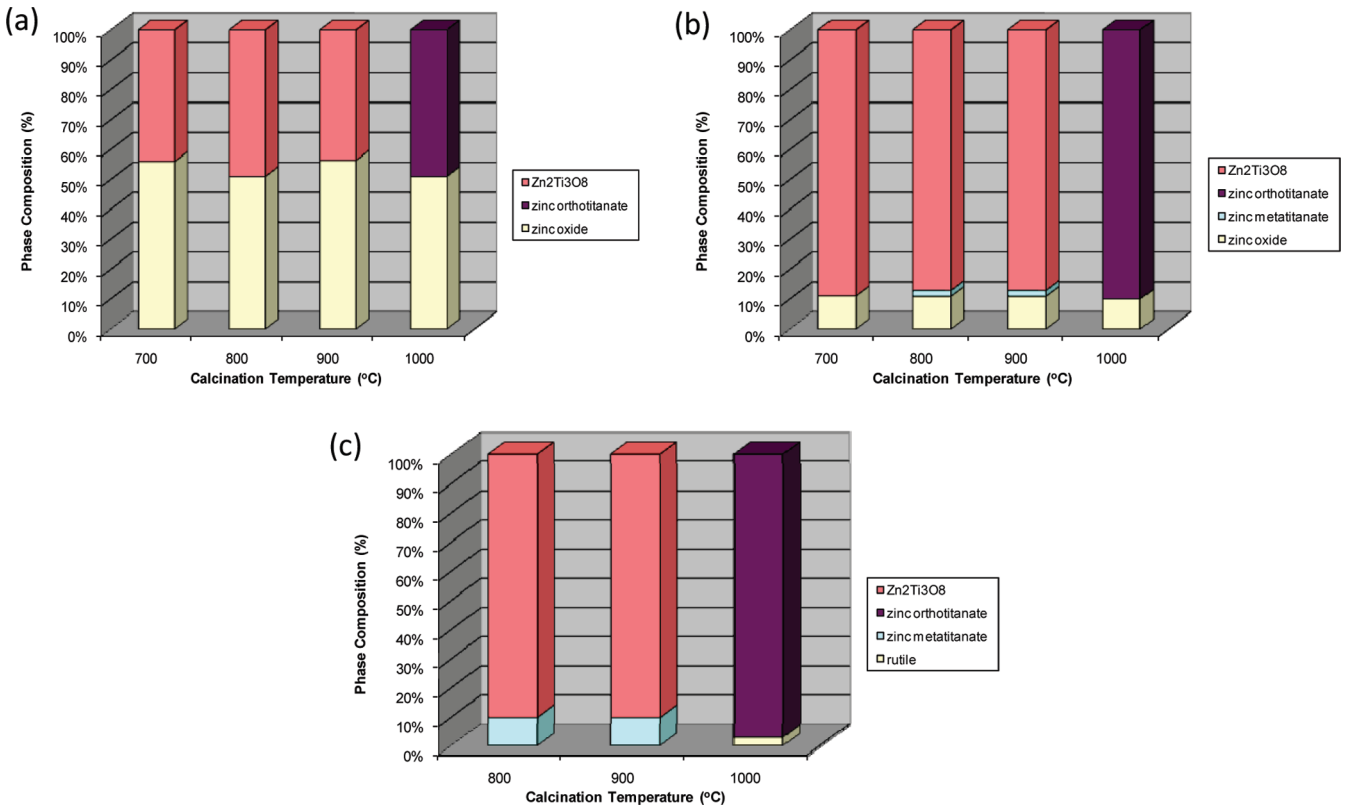

Figure 6. Phase composition of (a) sample TZ-1:4, (b) sample TZ-2:4, and (c) sample TZ-3:4.

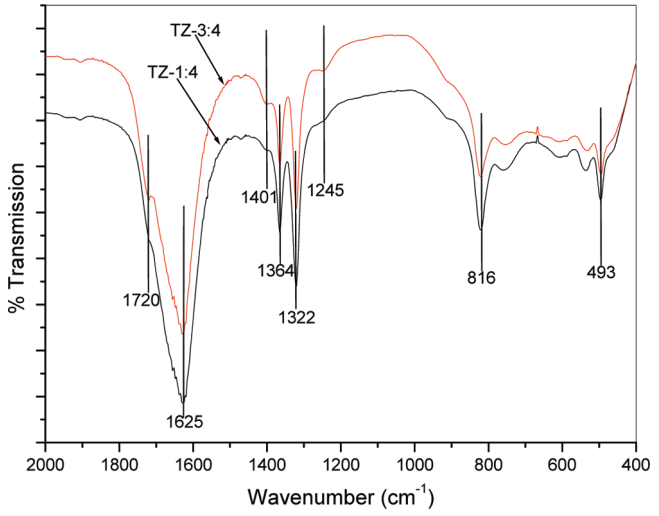

Figure 7. Infrared (IR) spectra of samples TZ-1:4 and TZ-3:4.

precursor is in excess over the amount of titanium; this behavior is adherently different from that of the excess titanium system, where results showed that zinc metatitanate transformed to zinc orthotitanate. Since this synthesis is not a typical solid-state reaction but rather a sol−gel reaction of titanium and zinc precursors, it is necessary to understand if the amorphous metal oxide structure influences the final crystalline structure. To determine the atomic arrangement of the metal oxide system in the early stages of the reaction, FTIR and Raman spectroscopic techniques were carried out on the samples before calcination.

Infrared Spectroscopy. When excess titanium is present, XRD has shown that, at low calcination temperatures (400−600 °C), anatase TiO_2 is favored over zinc oxide and, at higher temperatures (700−1000 °C), rutile TiO_2 dominates while zinc metatitanate transforms to zinc orthotitanate between 900 and 1000 °C.

The IR spectra of samples TZ-1:4 and TZ-3:4 are shown in Figure 7, with the peaks of interest labeled. For sample TZ-1:4, peaks at 1720 and 1401, 1245 cm^{-1}, which represent COO^-_{asym} and COO^-_{sym} of titanium oxalate, respectively, are significantly decreased when compared with the spectra of sample TZ-4:1 (see Figure 2). However, as the titanium ratio increases (sample TZ-3:4), peaks at 1720, 1401, and 1245 cm^{-1} appear, indicating the presence of titanium oxalate in the metal oxalate chain. Peaks at 816 and 493 cm^{-1}, representing δ_{asym}(O−C−O) and ν(M−O), δ_{asym}(C−C−O), respectively, are more intense for sample TZ-1:4 than for sample TZ-3:4. In the presence of greater amounts of zinc precursor, zinc oxalate dominates the metal oxalate chain network.

Symmetric and asymmetric carboxylate stretches from titanium and zinc oxalate are clearly present in the IR spectra shown. As expected, when the zinc precursor is in excess, carboxylate stretches of titanium oxalate are weak. However, when titanium is in excess, strong signals representative of zinc oxalate are still clear. This can be explained through the synthesis where zinc acetate is first reacted with oxalic acid to give zinc oxalate before titanium isopropoxide is added. Therefore, TTIP can chelate with unreacted oxalic acid.

Raman Spectroscopy. The Raman spectra of excess zinc samples TZ-1:4, TZ-2:4, and TZ-3:4 is shown in Figure 8. Peaks representative of the anatase four-peak pattern[33−35] are present at 155, 415, 545, and 615 cm^{-1}. All other signals in the region of 0−1000 cm^{-1} are believed to be caused by Zn−O contributions.

dx.doi.org/10.1021/cm1031688 |*Chem. Mater.* 2011, 23, 1496–1504

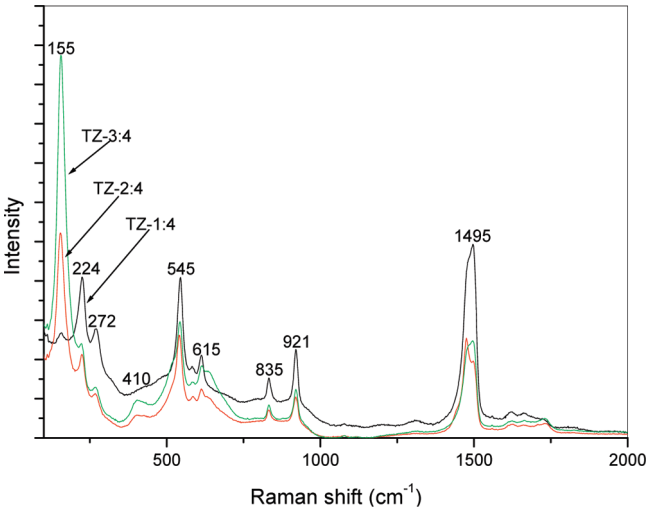

Figure 8. Raman spectra of samples TZ-1:4, TZ-2:4, and TZ-3:4.

There is a large signal at 1495 cm^{-1} that is due to $(COO^{-})_{sym}$ stretching of the oxalate group. Comparing the peak intensities of 1495 cm^{-1} with M−O peaks, this signal clearly is the largest, relative to its surrounding peaks for sample TZ-1:4, and, as the titanium ratio increases, the carboxylate peak decreases. Again, this is evidence of the dominant effect of zinc oxalate in the metal oxalate chain. The Raman spectra of samples TZ-2:4 and TZ-3:4 give similar peak positions to each other but the spectral profile of sample TZ-1:4 gives a spectrum that contains no similarities with either sample TZ-2:4 or sample TZ-3:4. In the spectra of samples TZ-2:4 and TZ-3:4, the increased levels of titanium lead to signals at 155, 415, 545, and 615 cm^{-1}, but the spectrum of sample TZ-1:4 does display these peaks. Therefore, all peaks shown in the spectrum of sample TZ-1:4 (see Figure 8) arise from Zn−O stretches.

The presence of the highlighted peaks show the dominant influence of the titanium as the ratio is increased. Comparison of Figure 3 with Figure 8 also shows that Ti−O bonds give exceptionally higher Raman signals than Zn−O bonds. There are no similarities between the peak profiles of the Raman and IR spectra. This suggests that the rule of mutual exclusion may be applied to the titanium−zinc oxalate structures.[36] Applying the rule of mutual exclusion would give a centrosymmetric structure, where the metal atoms occupy a position equidistant from the coordinating oxygens.[36] Summarizing the spectroscopic results:

- Oxalic acid chelates to titanium to form titanium oxalate
- Increasing zinc oxalate causes a reduction in asymmetric and symmetric carboxylate stretches from titanium oxalate and an increase in the symmetric stretch in Raman spectra
- When Ti is in excess, the anatase four-peak pattern dominates the Raman spectra, and there is a broad signal without significant individual peak contributions in IR (400−1000 cm^{-1})
- When Zn is in excess, the four-peak pattern is reduced in Raman spectra, and the IR spectra show individual peaks representative of O−C−O and M−O from zinc oxalate
- There is a metal oxalate chain composed of titanium and zinc
- In IR spectra, asymmetric and symmetric carboxylate stretches for zinc oxalate are always present, but carboxylate stretches are only present for titanium oxalate at high ratios

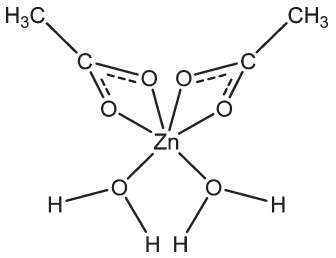

Figure 9. Molecular structure of zinc acetate dihydrate.

- The rule of mutual exclusion can be applied, indicating the presence of a symmetric molecule

DISCUSSION

Ishioka et al. showed the structure of zinc acetate dihydrate (see Figure 9) through X-ray crystallography.[37]

Reacting oxalic acid with zinc acetate forms the intermediate zinc oxalate (see reaction *R1*), as presented by Kanade et al.[38]

$$Zn(CH_3COO)_2\cdot 2H_2O_{(l)} + H_2C_2O_{4(l)} \rightarrow ZnC_2O_4\cdot 2H_2O_{(s)} + 2AcOH_{(l)} + 2H_2O_{(l)} \quad (R1)$$

X-ray crystallographic studies of zinc oxalate show that zinc is octahedrally coordinated to six oxygen atoms,[39,40] as shown in Figure 10a. Divalent metal cations and oxalate groups generate an infinite chain arrangement, as depicted in Figure 10b.[41,42]

Thermal treatment of zinc oxalate leads to the formation of zinc oxide. Thermogravimetric analysis/differential thermal analysis (TGA/DTA) studies have shown the removal of water at 120 °C and the decomposition of zinc oxalate at 400 °C, as shown in reaction *R2*.[38]

$$ZnC_2O_4\cdot 2H_2O_{(s)} + \frac{1}{2}O_{2(g)} \rightarrow ZnO_{(s)} + 2CO_{2(g)} + 2H_2O_{(l)} \quad (R2)$$

The system under investigation in this study is not zinc oxalate alone: it also includes varying ratios of titanium isopropoxide (see Figure 11a), which consists of monomeric units.[43] Previous reports have shown the chelation of acetic acid,[44,45] formic acid,[46] and acetyl acetone[47] to form titanium isopropoxide. As was shown with zinc oxalate,[41,42] titanium isopropoxide also forms chains upon reaction with a chelating agent (see Figure 11b).[48−50]

During the sol−gel reaction of titanium alkoxides, the OR groups are preferentially hydrolyzed while the ligands remain tightly bound throughout much of the condensation process, thus promoting the formation of linear chains of Ti−O polymers composed of edge-sharing octahedra.[45,51] The formation of these octahedra stabilizes TiO_2 as anatase, reducing the anatase-to-rutile transformation temperature.[45,51]

Previous research has shown the structure of zinc oxalate[39,40] and titanium carboxylates.[44−46] However, to the best of the authors' knowledge, a combination of structures has not been investigated previously. IR and Raman results have shown the presence of both titanium and zinc oxalate (see Figure 12), but it cannot be shown if titanium oxalate chains exist separately from zinc oxalate chains or do they combine. X-ray diffraction (XRD) results showed that initially crystalline ZnO or TiO_2 anatase formed separately, and, at higher calcination temperatures, zinc titanates were formed. This indicates that two separate metal

dx.doi.org/10.1021/cm1031688 |*Chem. Mater.* 2011, 23, 1496–1504

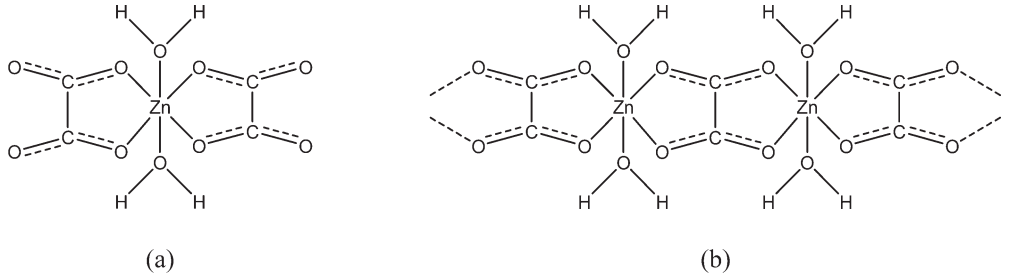

Figure 10. Molecular structure of (a) zinc oxalate dihydrate and (b) the infinite chain arrangement.

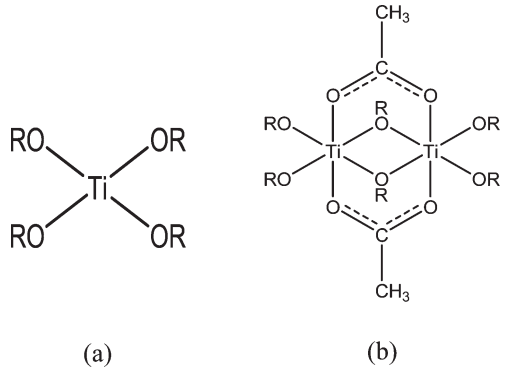

Figure 11. Molecular structure of titanium isopropoxide (a) chelated titanium isopropoxide (b).

oxalate chains were formed during the synthesis (see Figures 12a and 12b).

As the condensation process proceeds with excess titanium (TZ-4:1), TiO_6 octahedra form anatase-TiO_2 and ZnO_4 tetrahedra form ZnO (wurtzite). As the calcination temperature becomes more intense (≥600 °C), the TiO_6 octahedra and ZnO_4 tetrahedra undergo molecular rearrangement and phase transformation occurs. Zinc oxide tetrahedra and TiO_6 octahedra undergo further movement and combine to form zinc titanates and rutile. The metastable zinc metatitanate and stable rutile exist at 800 and 900 °C, with trace amounts of $Zn_2Ti_3O_8$ also being present. At 1000 °C, zinc metatitanate and $Zn_2Ti_3O_8$ decompose to form zinc orthotitanate, and rutile remains the dominant phase. As the amount of zinc precursor increases (samples TZ-4:2 and TZ-4:3), the crystals behave in a similar manner but with increasing amounts of zinc oxide at early calcination temperatures (400 and 500 °C) and greater amounts of zinc titanates at temperatures of ≥700 °C. The results (see Figures 1a−c) show that the percentage of zinc titanate at 700 °C is very similar to the final percentage of zinc orthotitanate. The results have shown that, at temperatures of 700−900 °C, for samples with excess titanium precursor, zinc metatitanate is the dominant zinc titanate phase and is stable up to 900 °C; it then undergoes complete transformation to form zinc orthotitanate. Phase transformation from zinc metatitanate to zinc orthotitanate is almost 100%; however, results do show that rutile is also formed. Calculated values for percentage conversion are 90% for sample TZ-4:1, 93% for sample TZ-4:2, and 98% for sample TZ-4:3, reflecting an increase in conversion that is consistent with increasing zinc precursor ratio.

Three different molar ratios where zinc precursors are in excess over titanium were also prepared. All three behaved differently than those where titanium was in excess. For all samples where zinc is in excess, accurate compositions at calcination temperatures of 400−600 °C could not be obtained from the X-ray diffractograms, because the peaks were not resolved; however, from the diffractograms, zinc oxide was determined to be the dominant phase at early temperatures, with anatase also being present in trace amounts. However, the percentage composition was calculated from results for temperatures of 700 °C onward (see Figures 6a, 6b, and 6c). When titanium was in excess, a clear transformation of large compositions of zinc metatitanate to zinc orthotitanate was noticed (40%, 60%, and 80% for samples TZ-4:1, TZ-4:2, and TZ-4:3, respectively). With excess zinc, zinc metatitanate is not present in sample TZ-1:4, for sample TZ-2:4, trace amounts of zinc metatitanate (2%) are present at 800 and 900 °C; and as the titanium ratio increases (sample TZ-3:4), larger amounts of zinc metatitanate (10%) are present at calcination temperatures 800 and 900 °C. With excess zinc, $Zn_2Ti_3O_8$ was the dominant metastable phase formed at temperatures of 700−900 °C; total phase transformation occurred at temperatures of >900 °C and zinc orthotitanate was formed. Unlike the excess titanium system, where zinc metatitanate transformed to zinc orthotitanate and rutile, with conversion percentages of 90%−98%, when zinc was in excess, it was $Zn_2Ti_3O_8$ combining with zinc oxide transforming to zinc orthotitanate. Conversion percentages of $Zn_2Ti_3O_8$ of >100% were calculated for samples TZ-1:4 (104%), TZ-2:4 (101%), and TZ-3:4 (107%); values of >100% are achieved because, unlike zinc metatitanate, which transforms to zinc orthotitanate and rutile, when zinc precursor is used in excess, $Zn_2Ti_3O_8$ is the favored phase, which combines with zinc oxide to form zinc orthotitanate.

The structures of all zinc titanates studied here share common features: they all consist of TiO_6 octahedra that are connected over common edges.[30] Anatase displays similarities with the spinel structures of Zn_2TiO_4 and $Zn_2Ti_3O_8$, but $ZnTiO_3$ shares its structure with rutile.[30,52] The formation of Zn_2TiO_4 and $Zn_2Ti_3O_8$ is limited by the presence of anatase and $ZnTiO_3$ only forms in the presence of rutile.[11,53] However, other researchers have shown that this is not necessarily the case.[27,30,53] Results from the present study show that, for samples where titanium is in excess (samples TZ-4:1, TZ-4:2, and TZ-4:3), anatase and zinc oxide are present during the early stages of crystallization (400−600 °C) and as the calcination temperature increases, zinc metatitanate is formed, and greater amounts of metatitanate are formed with an increased percentage of zinc oxide. These results suggest that, in a sol−gel synthesis, the formation of zinc metatitanate is determined not only by the presence of titanium dioxide (anatase or rutile) but also by the presence of zinc oxide. With excess zinc precursor (samples TZ-1:4, TZ-2:4, and TZ-3:4), zinc oxide was the dominant crystalline phase for calcination temperatures of 400−600 °C and as the temperature

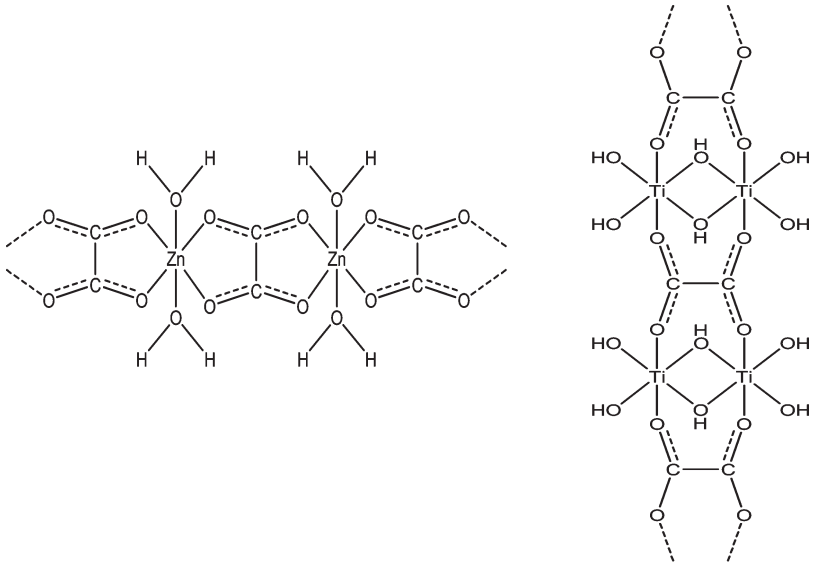

Figure 12. Proposed structures of metal oxalate chains formed: zinc oxalate (a) and titanium oxalate (b).

increased, $Zn_2Ti_3O_8$ became the dominant phase, transforming to zinc orthotitanate at 1000 °C, providing further evidence that anatase is not necessary for the formation of $Zn_2Ti_3O_8$ and that the percentage of zinc oxide influences which zinc titanate phase is formed.

CONCLUSIONS

A series of zinc titanate powders was successfully synthesized using a simple sol−gel technique. The effect of varying ratios of zinc/titanium precursors was investigated. The powders were calcined at temperatures in the range of 400−1000 °C, and the crystalline phases of the powders were determined using X-ray diffraction (XRD).

To determine the molecular structures of the samples before they underwent calcination, infrared and Raman spectroscopy were employed. Possible structures of zinc oxalate and titanium oxalate were proposed, based on spectroscopic results obtained and information known from the literature. Both the titanium oxalate and the zinc oxalate remain separate throughout the reaction, which may be shown through XRD results of the powders calcined at low temperatures (400 and 500 °C).

When the titanium precursor is in excess over the zinc precursor, formation of the metastable zinc metatitanate is favored, which ultimately transforms (90%−98% conversion) to zinc orthotitanate (<900 °C), with the presence of rutile from 700 °C onward. When zinc oxide is the dominant structure during the early stages of crystallization (400 and 500 °C), $Zn_2Ti_3O_8$ is the zinc titanate phase preferentially formed as the calcination temperature increases. Transformation of $Zn_2Ti_3O_8$ to zinc orthotitanate occurs at 1000 °C. Calculated crystallite size results showed that anatase/ZnO particle size did not influence the phase-transformation behavior of the materials.

AUTHOR INFORMATION

Corresponding Author

*E-mail: suresh.pillai@dit.ie.

ACKNOWLEDGMENT

The authors wish to thank the EPA for funding and the FOCAS Institute DIT and CREST-DIT for resources and materials. The authors would like to thank the CREST Centre Director, Dr. John Colreavy, for reviewing the manuscript.

REFERENCES

(1) Fujishima, A.; Honda, K. *Nature* **1972**, 238.
(2) O'Regan, B.; Gratzel, M. *Nature* **1991**, *353*, 737–740.
(3) Fox, M. A.; Dulay, M. T. *Chem. Rev.* **1993**, *93*, 341–357.
(4) Hoffmann, M. R.; Martin, S. T.; Choi, W.; Bahnemann, D. W. *Chem. Rev.* **1995**, *95*, 69–96.
(5) Kuo, Y.-L.; Chen, H.-W.; Ku, Y. *Thin Solid Films* **2007**, *515*, 3461–3468.
(6) Yu, J.; Yu, H.; Ao, C. H.; Lee, S. C.; Yu, J. C.; Ho, W. *Thin Solid Films* **2006**, *496*, 273–280.
(7) Kluth, O.; Schope, G.; Hupkes, J.; Agashe, C.; Muller, J.; Rech, B. *Thin Solid Films* **2003**, 442.
(8) Choi, W. S.; Kim, E. J.; Seong, S. G.; Kim, Y. S.; Park, C.; Hahn, S. H. *Vacuum* **2009**, *83*, 878–882.
(9) Zhang, Q.; Zhang, S.; Xie, C.; Fan, C.; Bai, Z. *Sens. Actuators B* **2008**, 128.
(10) Georgekutty, R.; Seery, M. K.; Pillai, S. C. *J. Phys. Chem. C* **2008**, *112*, 13563–13570.
(11) Bartram, S. F.; Slepetys, R. A. *J. Am. Ceram. Soc.* **1961**, *44*, 493–499.
(12) Dulin, F. H.; Rase, D. E. *J. Am. Ceram. Soc.* **1960**, *43*, 125–131.
(13) Mohammadi, M. R.; Fray, D. J. *J. Eur. Ceram. Soc.* **2010**, *30*, 947–961.
(14) Yamaguchi, O.; Morimi, M.; Kawabata, H.; Shimizu, K. *J. Am. Ceram. Soc.* **1987**, *70*, C97–C98.
(15) Chaves, A. C.; Lima, S. J. G.; Araujo, R. C. M. U.; Maurera, M. A. M. A.; Longo, E.; Pizani, P. S.; Simoes, L. G. P.; Soledade, L. E. B.; Souza, A. G.; dos Santos, I. M. G. *J. Solid State Chem.* **2006**, *179*, 985–992.
(16) Alonso, L.; Palacios, J. M.; Moliner, R. *Energy Fuels* **2001**, *15*, 1396–1402.
(17) Jothimurugesan, K.; Gangwal, S. K. *Ind. Eng. Chem. Res.* **1998**, *37*, 1929–1933.
(18) Jun, H. K.; Lee, T. J.; Ryu, S. O.; Kim, J. C. *Ind. Eng. Chem. Res.* **2001**, *40*, 3547–3556.

(19) Lew, S.; Sarofim, A. F.; Flytzani-Stephanipoulos, M. *Chem. Eng. Sci.* **1992**, *47*, 1421–1431.
(20) Pineda, M.; Fierro, J. L. G.; Palacios, J. M.; Cilleruelo, C.; Garcia, E.; Ibarra, J. V. *Appl. Surf. Sci.* **1997**, *119*, 1–10.
(21) Slimane, R. B.; Abbasian, J. *Adv. Environ. Res.* **2000**, *4*, 147–162.
(22) Jang, J. S.; Borse, P. H.; Lee, J. S.; Lim, K. T.; Jung, O.-S.; Jeoung, E. D.; Bae, J. S.; Won, M. S.; Kim, H. G. *Bull. Korean Chem. Soc.* **2009**, *30*, 3021–3024.
(23) Matsumoto, Y. *J. Solid State Chem.* **1996**, 126.
(24) Kim, H. T.; Byun, J. D.; Kim, Y. S. *Mater. Res. Bull.* **1998**, *34*, 963–973.
(25) Li, C.; Bando, M.; Nakamura, M.; Kimizuka, N.; Kito, H. *Mater. Res. Bull.* **2000**, *35*, 351–358.
(26) Sedpho, S.; Wongratanaphisan, D.; Mangkorntong, P.; Mangkorntong, N.; Choopun, S. *J. Nat. Sci.* **2008**, *7*, 99–104.
(27) Yang, J.; Swisher, J. H. *Mater. Charact.* **1996**, *37*, 153–159.
(28) Patterson, A. L. *Phys. Rev.* **1939**, *56*, 978–982.
(29) Scherrer, P. *Gottinger Nachrichten Gesell.* **1918**, *2*, 98.
(30) Liu, Z.; Dongxiang, Z.; Gong, S.; Li, H. *J. Alloys Compd.* **2009**, *475*, 840–845.
(31) Gabal, M. A.; El-Bellihi, A. A.; El-Bahnasaway, H. H. *Mater. Chem. Phys.* **2003**, *81*, 174–182.
(32) Doeuff, S.; Henry, M.; Sanchez, C.; Livage, J. *J. Non-Cryst. Solids* **1987**, *89*, 206–216.
(33) Hwang, D. S.; Lee, N. H.; Lee, D. Y.; Song, J. S.; Shin, S. H.; Kim, S. J. *Smart Mater. Struct.* **2006**, *15*, S74–S80.
(34) Kittaka, S.; K., M.; Takahara, S. *J. Solid State Chem.* **1997**, *132*, 447–450.
(35) Yoshitake, H.; Abe, D. *Microporous Mesoporous Mater.* **2009**, *119*, 267–275.
(36) Edwards, H. G. M.; Russell, N. C. *J. Mol. Struct.* **1998**, *443*, 223–231.
(37) Ishioka, T.; Shibata, Y.; Takahashi, M.; Kanesaka, I.; Kitagawa, Y.; Nakamura, K. T. *Spectrochim. Acta, Part A* **1998**, *54*, 1827–1836.
(38) Kanade, K. G.; Kale, B. B.; Aiyer, R. C.; Das, B. K. *Mater. Res. Bull.* **2006**, *41*, 590–600.
(39) Natarajan, S. *Solid State Sci.* **2002**, *4*, 1331–1342.
(40) Vaidhyanathan, R.; Natarajan, S.; Rao, C. N. R. *J. Chem. Soc., Dalton Trans.* **2001**, 699–706.
(41) D'Antonio, M. C.; Mancilla, N.; Wladimirsky, A.; Palacios, D.; Gonzalez-Baro, A. C.; Baran, E. J. *Vib. Spec.* **2010**, *53*, 218−221.
(42) Lagier, J. P.; Pezerat, H.; Dubernat, J. *Rev. Chim. Miner.* **1969**, *6*, 1081–1093.
(43) Bradley, D. C.; Mehrotra, R. C.; Gaur, D. P. *Metal Alkoxides*; Academic Press: London, 1978.
(44) Brinker, C. J.; Scherer, G. W. *The Physics and Chemistry of Sol−Gel Science*; Academic Press: New York, 1990.
(45) Nguyen, T.-V.; Choi, D.-J.; Yang, O.-B. *Res. Chem. Intermed.* **2005**, *31*, 483–491.
(46) Nolan, N. T.; Seery, M. K.; Pillai, S. C. *J. Phys. Chem. C* **2009**, *113*, 16151–16157.
(47) Phule, P. P.; Risbud, S. H. *J. Mater. Sci.* **1990**, *25*, 1169–1183.
(48) Doeuff, S.; Henry, M.; Sanchez, C.; Livage, J. *J. Non-Cryst. Solids* **1987**, *89*, 206−216.
(49) Mehrotra, R. C.; Bohra, R. *Metal Carboxylates*; Academic Press: London, 1983.
(50) Yoldas, B. E. *Am. Ceram. Soc. Bull.* **1975**, 54.
(51) Livage, J.; Sanchez, C.; Henry, M.; Doeuff, S. *Solid State Ionics* **1989**, *32/33*, 633–638.
(52) Sugiura, M.; Ikeda, K. *J. Jpn. Ceram. Assoc.* **1947**, *55*, 62–66.
(53) Kim, H. T.; Kim, S. H.; Nahm, S.; Byun, J. D.; Kim, Y. *J. Am. Ceram. Soc.* **1999**, *82*, 3043–3048.